A Novel Wet-Etching Method Using Electric-Field-Assisted Proton Exchange in $LiNbO_3$

Tzyy-Jiann Wang, *Member, IEEE*, Chih-Feng Huang, Way-Seen Wang, *Member, IEEE*, and Pei-Kuen Wei

***Abstract*—This paper presents a novel wet etching method for $LiNbO_3$ using electric-field-assisted proton exchange. By applying voltage with appropriate polarity on designed electrodes placed on both sides of substrate, the induced electric-field distribution can effectively suppress or enhance proton diffusion in the lateral and depth directions. Thus, the proton-exchanged range in $LiNbO_3$ can be expertly manipulated. Because the proton-exchanged region can be removed by using a mixture of HF/HNO_3 acids, the proposed wet-etching method can effectively control the shape of the etched region in the $LiNbO_3$ substrate. Under appropriate electrode and proton-exchange parameters, a vertical sidewall with smooth surface is successfully produced, which makes fabricating reflection mirrors and T-junctions in $LiNbO_3$ possible. By utilizing the proposed wet-etching method, optical integrated circuits with higher integration density can be fabricated in $LiNbO_3$.**

***Index Terms*—Integrated optics, lithium niobate, proton exchange, waveguide mirror.**

I. Introduction

FABRICATION of optical integrated circuits with high performance and high integration density is the goal that many researchers in the realm of integrated optics pursue. Highly integrating various devices in a single chip not only makes chips possess new and diversified functions, but also enhances the overall performance and its application range. In order to increase integration density, various waveguide structures, such as right-angle bend [1]–[12], T-junction [11]–[13], and photonic crystal [14], are proposed. To fabricate these structures requires using high-index-contrast materials and mature etching techniques to produce smooth and vertical etching surfaces. In silicon and III–V material systems, these requirements are satisfied, and the related devices have been successfully demonstrated. In lithium niobate ($LiNbO_3$), these devices cannot be fabricated due to the restriction of the present etching techniques. In this work, a new etching technique to solve this problem is proposed.

Manuscript received June 30, 2003; revised November 12, 2003. This work was supported by the National Science Council, Taipei, Taiwan, R.O.C., under Contracts NSC 91–2215-E-027–005 and NSC 92–2215-E-027–001.

T.-J. Wang and C.-F. Huang are with the Institute of Electro-Optical Engineering, National Taipei University of Technology, Taipei 10651, Taiwan, R.O.C.

W.-S. Wang is with the Department of Electrical Engineering, National Taiwan University, Taipei 10617, Taiwan, R.O.C.

P.-K. Wei is with the Institute of Applied Science and Engineering Research, Academia Sinica, Taipei 11564, Taiwan, R.O.C.

Digital Object Identifier 10.1109/JLT.2004.829229

Lithium niobate has excellent electrooptic, acoustooptic, piezoelectric, and nonlinear-optic properties. It is broadly employed to produce various devices and is an important material in integrated optics. In device fabrication processes, techniques of etching lithium niobate are frequently required to produce diverse structures, such as gratings and ridge devices. In addition, they are also needed to enhance the performance of high-frequency modulators. Due to its strong etching resistance, etching $LiNbO_3$ is difficult. Hence, developing a new etching technique with a high-etching-rate, smooth and vertical etching surface is an important research topic. Traditional dry-etching methods such as plasma etching [15], sputter etching [16], and reactive ion etching [17] have a very slow etching rate and produce a rough etching surface. Wet etching of lithium niobate using an HF/HNO_3 mixture initially is used to determine domain polarity and defect topology. This mixture only etches the negative z-face and leaves the positive z-face unchanged. By introducing structural defects in $LiNbO_3$, any exposed surface can be etched, and the etching rate rises notably. Based on the concept, Laurell *et al.* [18] proposed a new wet-etching method for $LiNbO_3$. They used a proton-exchange method to produce structural defects in specified regions and then removed them by an HF/HNO_3 mixture. A several-micrometer etching depth and a smooth etching surface can be obtained. By utilizing the method, ridge waveguides and the related devices on different crystal orientation of lithium niobate have been successfully produced [19]–[21]. However, due to the proton lateral diffusion in the proton-exchange process, the sidewall of the etched region has a slanted or curve shape, depending on the proton-exchange temperature and time [20].

In an optical integrated circuit, reflection mirror and T-junction are important components for compact lightwave steering. In order to reduce the reflection/splitting loss, the chosen etching method to produce these devices must satisfy several requirements.

1) They must generate a smooth etching surface to diminish the scattering loss.
2) They must create an adequate etching depth to reflect or split most of the optical field in the waveguide.
3) They must produce a vertical sidewall to reflect the optical field horizontally to the waveguide.

The effects of various mirror parameters [22]–[27], such as mirror roughness, mirror verticality, mirror lateral tilt, and mirror offset, on the device performance have been discussed in previous literature. For the practical mirror, mirror height

(or etching depth) must be larger than mode size to avoid the interference of mode field by mirror edge, and mirror surface roughness should be less than one tenth of the light wavelength to be optically smooth. The mirror tilt from verticality must be less than 4° in order to have a loss of less than 3 dB [27].

Though the dry-etching methods can produce a vertical sidewall, its surface quality and the etching depth are inadequate. The wet-etching method proposed by Laurell *et al.* does not have such drawbacks, but its nonvertical sidewall will reflect the optical field toward the substrate, not the waveguide, and results in a large reflection/splitting loss. Hence, restricted by the present etching techniques, the structures needed to reduce the device area in the chip and to increase integration density, such as right-angle bend and T-junction, cannot be fabricated in $LiNbO_3$. This limits the enhancement of the chip function and impedes the popularization of $LiNbO_3$ devices due to the difficulty in reducing the manufacture cost. In this paper, a new wet-etching method using electric-field-assisted proton exchange is proposed. By designing the electric-field distribution in the proton-exchange process, the etching profile of lithium niobate can be controlled. A smooth and vertical sidewall, which is suitable for fabricating right-angle bends and T-junctions, can be produced.

This paper is organized as follows. The design concept of the proposed wet-etching method using electric-field-assisted proton exchange is illustrated in Section II. The resultant electric-field distribution in the designed electrode structure is calculated, and the effect of structural parameters on electric-field distribution is discussed. The experimental setup, process, and the related problems are presented in Section III. The effect of benzoic acid placed on the side of the bottom electrode and the applied voltage on the etching profiles are discussed. Section IV provides a discussion about the results in simulations and experiments. The conclusion is given in Section V.

II. Design and Simulation

A. Principle

During the proton-exchange process, protons diffusing into lithium niobate not only move in a direction perpendicular to the substrate surface, but also diffuse laterally in the substrate inside. The proton lateral diffusion results in a proton-exchanged region, in a side view, with a slanted or curve-shaped boundary [20]. The incoming protons will induce structural defects in $LiNbO_3$, which can be easily removed by a mixture of HF/HNO_3 acids. When immersing the substrate in this mixture, only the proton-exchanged regions are etched. The revealed etching profile completely coincides with the boundary of the proton-exchanged region and has a slanted or curve-shaped sidewall. Hence, the conventional wet-etching method could not produce a vertical etching sidewall and is not suitable to be used in the fabrication process of reflection mirrors and T-junctions for reducing the area that the devices occupy in a chip.

The proton lateral diffusion results from a proton concentration gradient in the lateral direction. In order to suppress the lateral diffusion, an external force along the contradirection of the concentration gradient must be applied. In this paper, the required force is produced by the externally applied electric field,

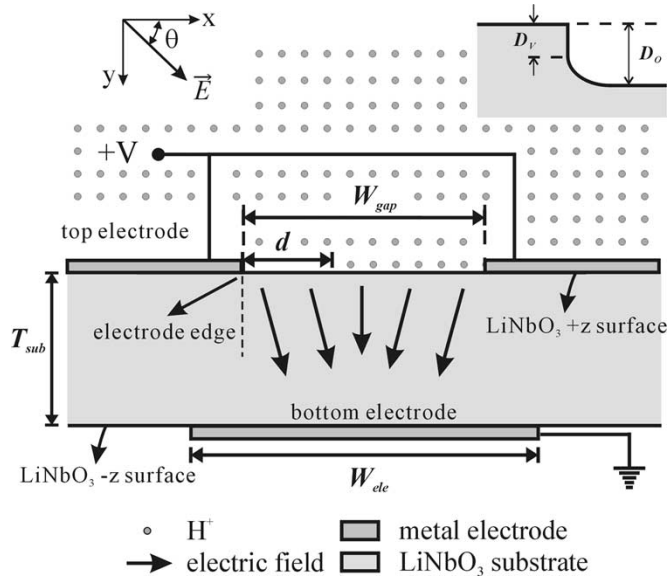

Fig. 1. Schematic diagram for the electric-field-assisted proton exchange with the designed electrodes. Inset: the upper left is the definition of the orientation angle of electric field, and the upper right is the resultant etching profile, where D_v and D_o denote the vertical sidewall depth and the overall etching depth, respectively.

which is formed by applying the voltage on the designed electrodes. The new electrode structure in the electric-field-assisted proton-exchange process is shown in Fig. 1. It is expected that for this electrode structure, the direction of the electric field near the edge of window opening is toward the center of window opening. It is opposite to the direction of concentration gradient and will have the effect of suppressing the proton lateral diffusion.

B. Calculation of Electric-Field Distribution

In order to understand the electric-field distribution in the substrate, the electrode analysis using the finite-element method [28] is conducted. In order to shorten the CPU time and decrease the computer memory requirement in simulation, a nonuniform mesh with denser grid points near the proton-exchanged region is used. The electrode structure in simulation, as shown in Fig. 1, has the following parameters: the gap between top electrodes $W_{\rm gap} = 20$ μm, the width of the bottom electrode $W_{\rm ele} = 150$ μm, the substrate thickness $T_{\rm sub} = 500$ μm, and the applied voltage $V = 100$ V. The electric-field vector distribution under the substrate surface corresponding to $y = 0$ is shown in Fig. 2. Near the edge of top electrodes, the electric field has a large horizontal component toward the center of the window opening, whose direction is contrary to the concentration gradient in the lateral direction, and can be used to suppress the proton lateral diffusion. The vertical component of the electric field exists everywhere beneath the substrate surface and has a maximum also near the edge of top electrodes. It is directed downward, and its effect on the protons is to accelerate them to reach the deeper region. Fig. 3 shows the electric-field distribution along the y direction at $d = 0, 1, 2, 3, 4, 5$ μm, where d is the distance from the top-electrode edge (refer to Fig. 1). The direction of the electric field is described by the angle relative to the x axis, as shown in the inset on the upper-left side of Fig. 1. The electric field is the strongest on the substrate surface

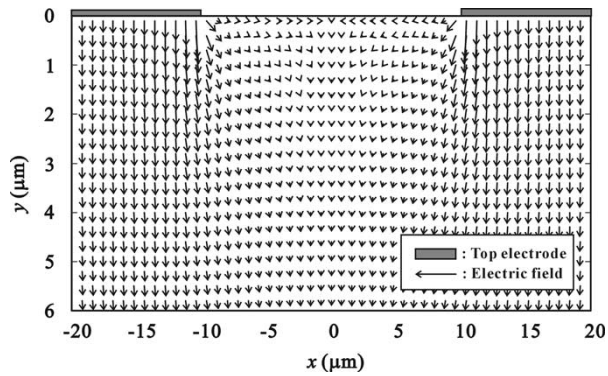

Fig. 2. Electric-field vector distribution beneath substrate surface with voltage $V = 100$ V applied on the proposed electrode structure with the parameters: $W_{\rm gap} = 20\ \mu$m, $W_{\rm ele} = 150\ \mu$m, and $T_{\rm sub} = 500\ \mu$m.

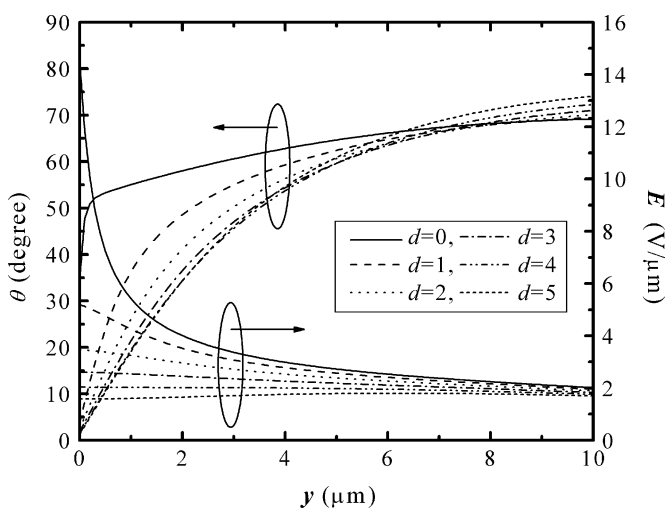

Fig. 3. Electric-field distribution (orientation angle θ and field value E) along the depth direction at the position $d = 0, 1, 2, 3, 4, 5$ with the same parameters as that for Fig. 2.

and decreases with depth y and distance d. The electric field at the electrode edge has an orientation angle of $\theta = 34.3°$, which can direct the incoming protons to move in counterdirection of the concentration gradient. It is noted that the orientation angle θ has a value of $< 30°$ for $d \geq 1$, which means a larger force (E_x) to suppress proton lateral diffusion. In addition, even though the depth y increases to 10 μm, the electric field still has an orientation angle about 70°. Therefore, as the applied voltage is sufficiently large, the ability of the electric field to suppress the proton lateral diffusion can extend to a depth at least 10 μm, which means a potential to produce a mirror of height 10 μm. This mirror height is sufficient to reflect the most power of the optical field.

C. Effect of Structural Parameters on Electric-Field Strength

The range of the proton-exchanged region (after etching, it is the etching region) depends on the proton diffusion coefficient, the proton-exchange time, and the applied electric field. The proton-exchange depth can be controlled by varying proton diffusion coefficient (or proton-exchange temperature) and proton-exchange time. The only parameter that can control the proton-exchange lateral profile is the electric field. It can affect proton movement in the lateral and depth directions and can be used to control the overall proton-exchange profile. The electric-field strength and distribution is determined by the voltage value and the electrode structure used in the proton-exchange process. The E_x component controls the suppression level of proton lateral diffusion. The E_y component affects the rate of proton movement in the depth direction. The combination of E_x and E_y govern proton movement and, thus, the subsequent etching profile. Experimental results show that the resultant etching profile has a shape as shown in the inset on the upper-right side of Fig. 1, where D_v and D_o denote the vertical sidewall depth and the overall etching depth, respectively. The formation of the vertical sidewall is the result of the action balance between the applied E_x and the lateral concentration gradient. In the following, the effects of structural parameters, such as bottom-electrode width ($W_{\rm ele}$) and substrate thickness ($T_{\rm sub}$), on the resultant electric-field distribution are considered. Because lateral diffusion starts at the place right beneath the top-electrode edge, the variation of the electric field at this place with different depth, such as $y = 0, 1, 2, 3, 4, 5$, is observed. In the simulation, the gap between top electrodes $W_{\rm gap}$ is set as 100 μm, and the applied voltage V is 100 V.

Fig. 4(a) and (b) shows the variation of the electric field at different depth with $W_{\rm ele}$ for $T_{\rm sub} = 50$ and 500 μm. For $T_{\rm sub} = 50\ \mu$m, while $W_{\rm ele}$ increases, the orientation angle and the field value of electric field rise and gradually approach a constant when $W_{\rm ele} > 200\ \mu$m ($= 2W_{\rm gap}$). As expected, for $W_{\rm ele} < 2W_{\rm gap}$, the decrease of the bottom-electrode width has the effect of field concentration toward the center of window opening and results in a smaller orientation angle. While $W_{\rm ele}$ increases further beyond $2W_{\rm gap}$, the increasing part of the bottom electrode is far from the top-electrode gap. Hence, a greater increase in $W_{\rm ele}$ has a less influence on the electric-field distribution therein, and the electric field tends to be invariant. In addition, an obvious decay of the field value with depth is also observed. The counterpart for $T_{\rm sub} = 500\ \mu$m is shown in Fig. 4(b). When the substrate becomes thicker, the dependence of the electric field on $W_{\rm ele}$ vanishes, even for the electric field at a different depth. It is because a widened bottom electrode at a distance has less influence on the field distribution near the top-electrode gap.

Fig. 5 shows the dependence of the electric field on $T_{\rm sub}$ for $W_{\rm ele} = 400\ \mu$m, in the vicinity of which the electric field is invariant with $W_{\rm ele}$, as shown in Fig. 4(a). While $T_{\rm sub}$ increases, the orientation angle θ of the electric field slightly decreases and then approaches a constant. The slight decrease of θ is due to a larger decrease rate of E_y than that of E_x and a larger $W_{\rm ele}$ than $W_{\rm gap}$. As to the electric-field value, its decrease rate with $T_{\rm sub}$ is more obvious than that for θ, and it also has a saturated value for $T_{\rm sub} > 200\ \mu$m. This means that when the substrate can be thinner below 200 μm, the electric field will be effectively enhanced.

III. Experiment and Results

A. Fabrication Process

The proposed wet-etching method is realized on z-cut $LiNbO_3$. Fig. 6 illustrates the fabrication process. First, a 300-nm aluminum film is evaporated onto the negative z face. The pattern of the designed bottom electrode is transferred to the photoresist on the aluminum thin film by photolithography.

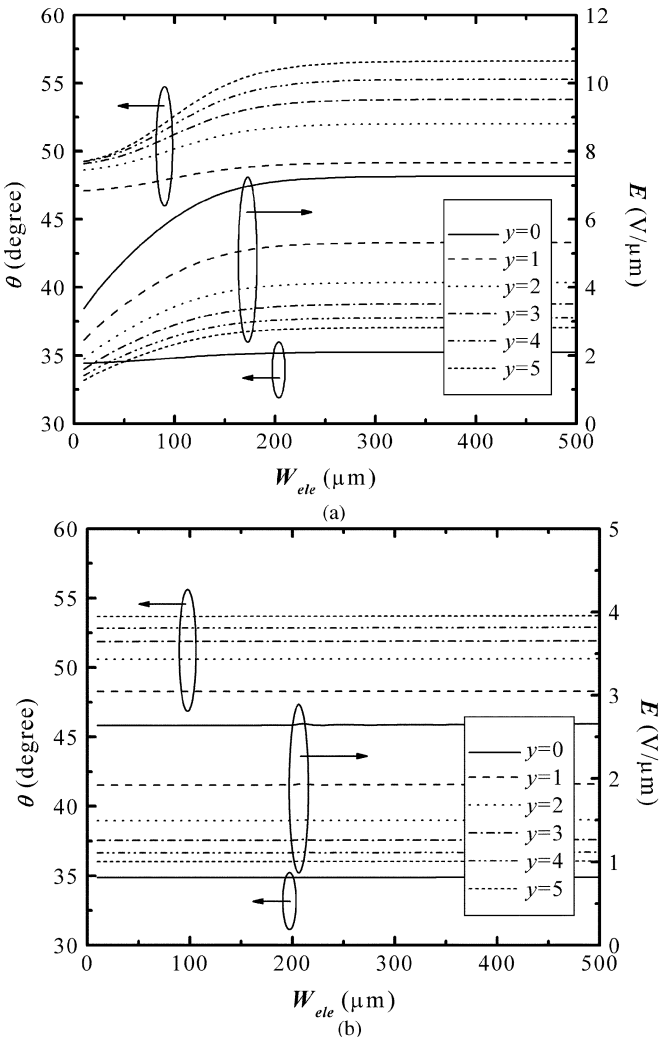

Fig. 4. Electric field (orientation angle θ and field value E) beneath the electrode edge at the depth $y = 0, 1, 2, 3, 4, 5$ versus bottom-electrode width $W_{\rm ele}$ for (a) $T_{\rm sub} = 50\ \mu$m and (b) $T_{\rm sub} = 500\ \mu$m, with parameters $W_{\rm gap} = 100\ \mu$m and $V = 100$ V.

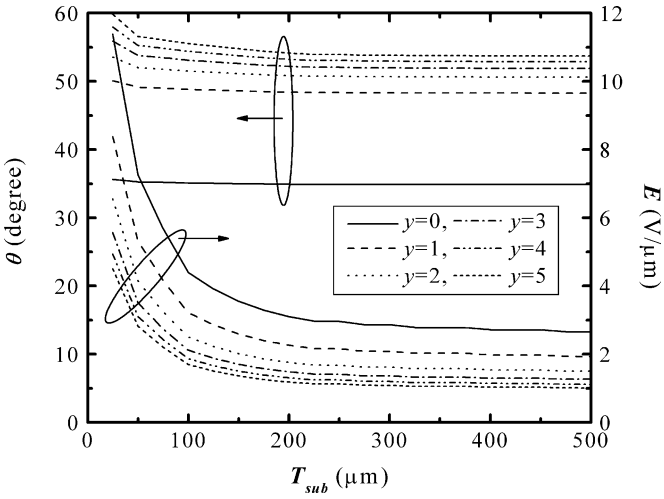

Fig. 5. Electric field (orientation angle θ and field value E) beneath the electrode edge at the depth $y = 0, 1, 2, 3, 4, 5$ versus substrate thickness $T_{\rm sub}$ with parameters $W_{\rm gap} = 100\ \mu$m, $W_{\rm ele} = 400\ \mu$m, and $V = 100$ V.

Then, the sample is immersed in the aluminum etching solution to remove the unwanted part. Thus, the bottom electrode is

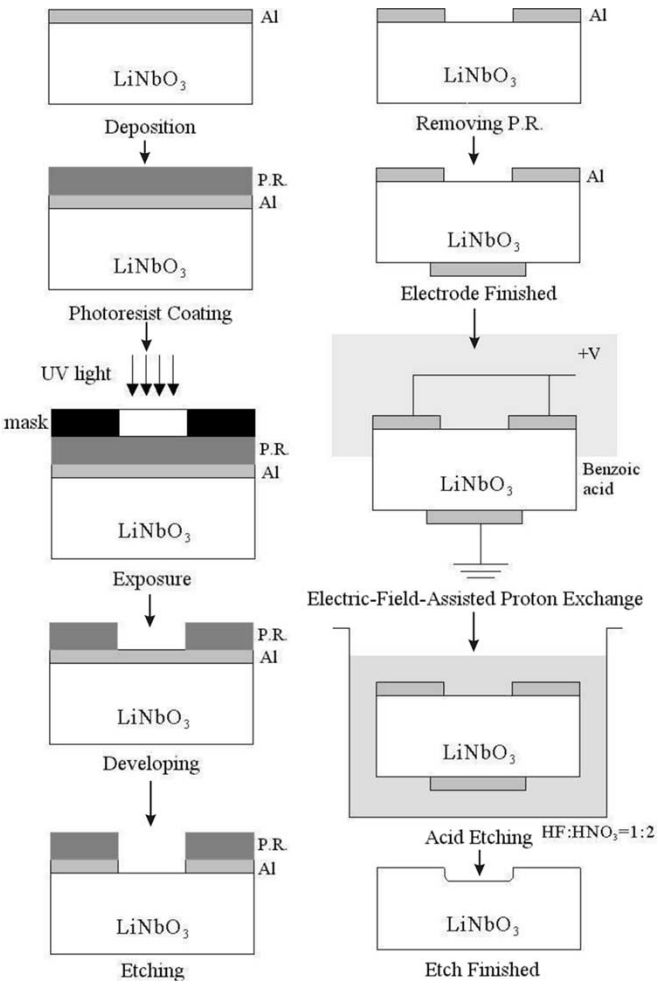

Fig. 6. Fabrication process for the proposed wet-etching method.

finished. Using the double-side mask aligner and following the same previous process, the top electrodes are fabricated and also can be used as the mask for proton exchange. Then, the sample is immersed in the benzoic acid, and the specific voltage is applied between the top and the bottom electrodes. The top electrode is connected to the positive terminal of the high-voltage power supply, and the bottom electrode is connected to the ground. It is noted that the top and the bottom electrodes must be separated and put in different melts of benzoic acid in order to avoid the strong oxidation-reduction reaction, which will result in the violent corrosion of both electrodes. Next, the temperature of benzoic acid is gradually raised to 240 °C and kept at this temperature for 4 h. After the electric-field-assisted proton-exchange process, the substrate is cleaned and then immersed in the mixture of HF and HNO_3 acids ($HF : HNO_3 = 1 : 2$) at room temperature for over 6 h to completely etch the proton-exchanged regions. In order to view the etching profile, the substrate is cut along the center of the etching region, and the revealed substrate side is polished for cross-sectional observation by a scanning electron microscope (SEM).

In the experiment, commercial optical-grade lithium niobate substrates of thickness ($T_{\rm sub}$) 500 μm are used. The gap between top electrodes ($W_{\rm gap}$) is set as 20 μm. Just as the simulation results show, the etching depth is almost independent of $W_{\rm ele}$

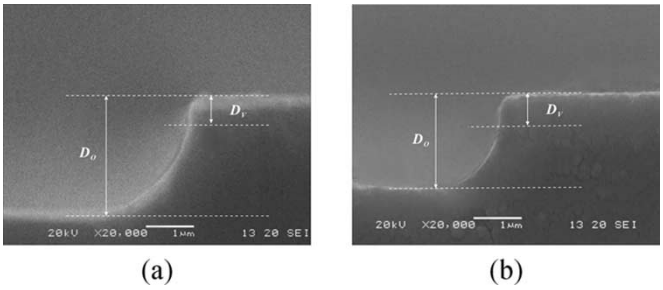

Fig. 7. SEM images of the etching profiles using the experiment setup (a) without benzoic acid and (b) with benzoic acid on the side of bottom electrode. The electric-field-assisted proton exchange is done at 240 °C for 4 h with the applied voltage of 100 V.

TABLE I
VERTICAL SIDEWALL DEPTH AND THE OVERALL ETCHING DEPTH FOR THE EXPERIMENTAL SETUP WITHOUT AND WITH BENZOIC ACID ON THE SIDE OF THE BOTTOM ELECTRODE (APPLIED VOLTAGE $V = 100$ V)

	No benzoic acid on the side of the bottom electrode	Benzoic acid on the side of the bottom electrode
Vertical sidewall depth	0.61 μm	0.69 μm
Overall etching depth	2.54 μm	2.0 μm

because the substrate is as thick as 500 μm. In the following, the experimental results for $W_{\rm ele} = 150$ μm are presented.

B. The Effect of Benzoic Acid on the Side of the Bottom Electrode

In the proton-exchange process, protons diffuse into the substrate and exchange with lithium ions in $LiNbO_3$. Then, lithium ions leave the substrate in a direction opposite to the proton moving direction and enter into the benzoic acid melt. Since protons and lithium ions are positively charged, in the electric-field-assisted proton-exchange process, the applied electric field will make them move in the same direction. In order to complete the proton-exchange process, the lithium ions must move more deeply into the substrate and find an exit in the other side in order to keep the substrate electrically neutral. As mentioned previously, the top and the bottom electrodes must be kept in different melts of benzoic acid to avoid the oxidation-reduction reaction. In order to carry out the electric-field-assisted proton exchange, the top electrodes must be immersed in the melt of benzoic acid.

Two experiments, with and without benzoic acid on the side of the bottom electrode, were conducted to test the previously stated hypothesis. The electric-field-assisted proton-exchange process proceeded at a temperature of 240 °C for 4 h with the applied voltage of 100 V. Fig. 7(a) and (b) shows the SEM images of the etching profile for two cases without and with benzoic acid on the side of the bottom electrode. The upper side of the etching sidewall is not so sharp because of the abrasion in the cut and polishing processes. The measured depths are shown in Table I. The vertical sidewall depth for the case with benzoic acid is somewhat larger than that for the case without benzoic acid. Hence, benzoic acid on the side of the bottom electrode indeed facilitates the moving out of the lithium ions and has a better effect on suppressing the proton lateral diffusion. As to the overall etching depth, the case without the benzoic acid is deeper than that with the benzoic acid. It is supposedly due to the extra-induced structure defect from the accumulation of lithium ions in the boundary of the proton-exchanged region. Since the short-circuit problem caused by the benzoic acid leakage between the top and the bottom electrodes at high temperature increases the difficulty in experiment, the setup without benzoic acid on the side of the bottom electrode is used in the following experiments.

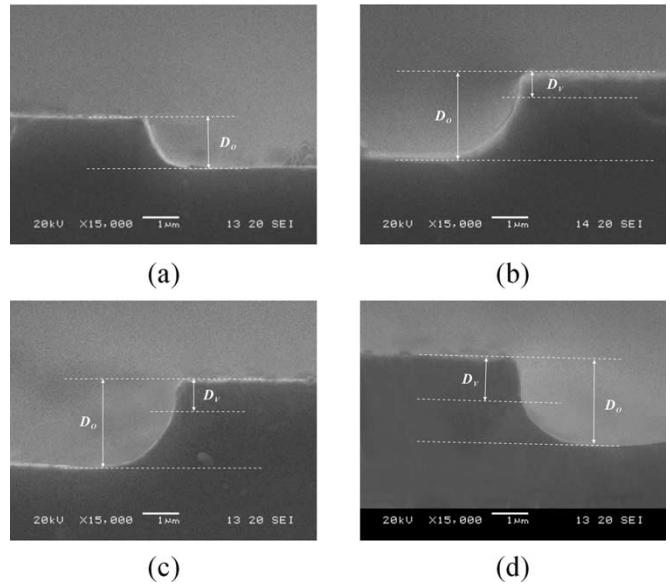

Fig. 8. SEM images of the etching profiles correspond to the applied voltage: (a) $V = 0$ V; (b) $V = 100$ V; (c) $V = 200$ V; (d) $V = 300$ V. The electric-field-assisted proton exchange is done at 240 °C for 4 h.

C. The Effect of Applied Voltage

The applied voltage determines the strength of the electric field to counteract the proton lateral diffusion caused by the concentration gradient. In order to understand the effect of applied voltage, the electric-field-assisted proton-exchange process is carried out at the temperature 240 °C for 4 h with applied voltage $V = 0$, 100, 200, and 300 V. The corresponding SEM images of the etching profiles are shown in Fig. 8. When no voltage is applied, the etched region has a slant-shaped sidewall, as shown in Fig. 8(a). When the voltage is applied on the electrodes, the etching profile near the substrate surface appears to be vertical, and the vertical sidewall depth is about 0.72 and 0.86 μm, corresponding to $V = 100$ and 200 V, as shown in Fig. 8(b) and (c). As the applied voltage increases to 300 V, the vertical sidewall depth reaches 1.23 μm, which is over one half of the overall etching depth (2.35 μm).

The root-mean-square roughness of the substrate surface is measured by an atomic force microscope (AFM) in the range of 5×5 μm. The AFM images of the plain $LiNbO_3$ substrate surface and of the $LiNbO_3$ substrate surface treated by the proposed wet-etching method are shown in Fig. 9. The root-mean-square roughness of the plain substrate surface is 0.430 nm. After etching by the proposed method, the roughnesses of the substrate surfaces are 1.767, 0.996, and 1.913 nm,

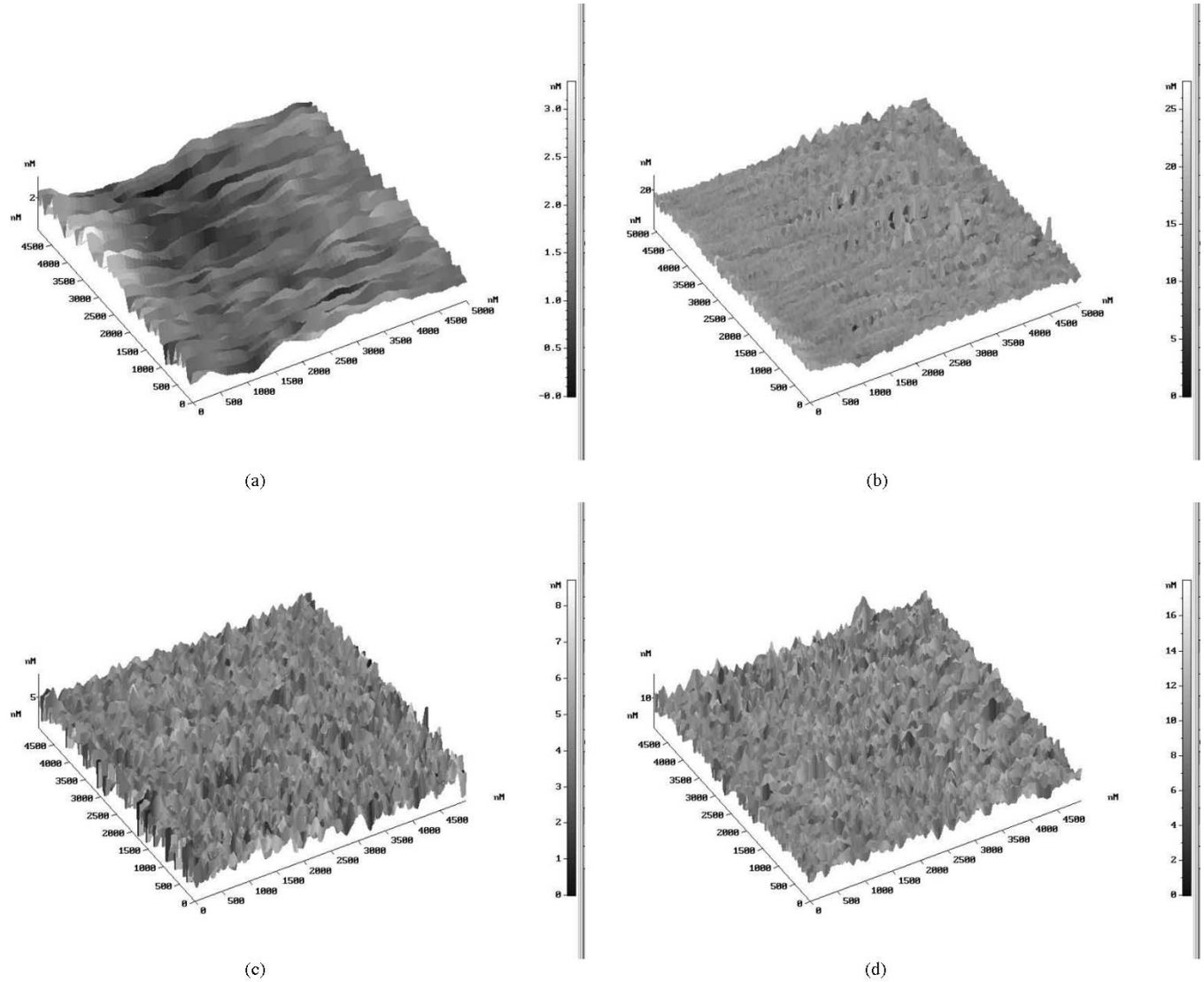

Fig. 9. (a) AFM image of plain $LiNbO_3$ substrate surface, and various AFM images of the $LiNbO_3$ substrate surfaces treated by the proposed etching method with the applied voltages: (b) $V = 0$ V; (c) $V = 100$ V; and (d) $V = 300$ V.

corresponding to the applied voltages $V = 0$, 100, and 300 V, respectively. It is found that the etched surfaces produced by the proposed method become slightly rougher. Even so, their roughness is still far less than one tenth of the light wavelength (for example, it is 63.28 nm for a light wavelength of 632.8 nm). Hence, their surfaces are optically smooth and can be used as the reflection mirror.

Fig. 10 shows the overall etching depth (D_o) and the vertical sidewall depth (D_v) versus the applied voltage V. As expected, with an increase in the applied voltage, the proton lateral diffusion is suppressed more effectively, and the vertical sidewall depth increases rapidly. When the applied voltage increases further, the increase rate of the vertical sidewall depth is not as large as the previous. It is supposedly due to the weaker electric field in the deeper region and the accumulation of lithium ion on the boundary of the proton-exchanged region caused by lack of benzoic acid on the side of bottom electrode. The repellence of the positives charges, which exists between protons and lithium ions, impedes the rapid increase of the vertical sidewall depth. As a whole, the larger the applied voltage, the larger the vertical sidewall depth. As to the overall etching depth, while the applied voltage increases, its value initially grows rapidly and

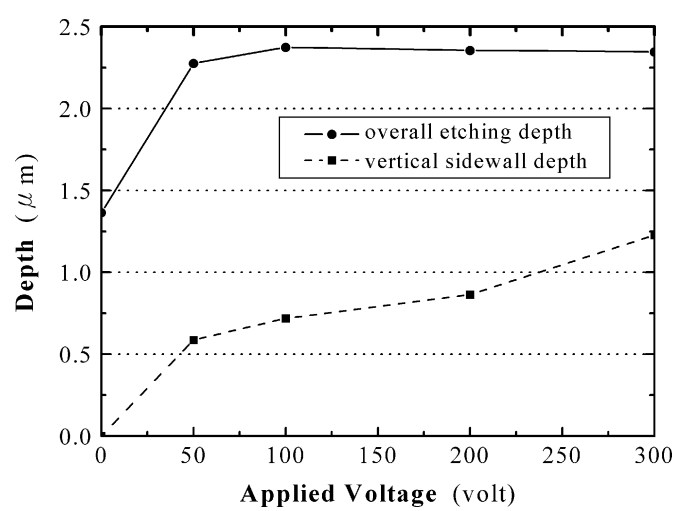

Fig. 10. Overall etching depth (D_o) and the vertical sidewall depth (D_v) versus the applied voltage.

then approaches a constant but with a slighter reduction. The causes of this variation are the same as that for the vertical sidewall depth. The overall etching depth with the applied voltage of 300 V has a 72.0% increase than that without applied voltage. Hence, the proposed wet-etching method not only creates a vertical sidewall with smooth surface, which has not been achieved by the present dry- and wet-etching techniques, but also effectively increases the overall etching depth, which will facilitate shortening the process time and reducing the manufacture cost.

IV. Discussion

When the voltage is applied on the electrodes, the electric-field distribution is set up in the substrate. Exactly beneath the electrode edge, there exists a critical depth such that the electric-field component E_x has a value, which can counteract the proton lateral diffusion caused by the concentration gradient. As the applied voltage increases, not only does E_x but also E_y have a larger field value. The increased E_x enhances the critical depth, and the larger E_y accelerates the proton diffusion rate in the depth direction. As the depth that the proton can reach is below this critical depth, the vertical sidewall depth increases with the applied voltage. Once beyond the critical depth, the vertically etching depth no longer increases with the applied voltage. In addition, as the applied voltage rises, the increase of the electric field in the deeper region is not so large as that in the shallow region, which results in a slower increase rate of critical depth with the applied voltage.

As shown in Fig. 3, the electric field at $d \geq 1$ has a smaller orientation angle ($\theta < 30^\circ$) than that at the electrode edge ($d = 0$). In other words, in this region, it has a larger E_x component, which can suppress proton lateral diffusion more effectively. Simulation results show that the maximum values of the electric-field component E_x at different depths appear around $d = 1$. In order to utilize this larger electric field, a nonconducting layer, such as silicon oxide, can be used as a mask for the proton exchange, instead of the original design in which the top electrodes are also used as a mask for proton exchange. This extra layer has a smaller window opening than the top-electrode gap in order to cover the substrate surface from $d = 0$ to $d = 1$. Thus, the incoming protons at the mask edge suffer the action of a large E_x, and therefore, a stronger suppression effect for proton lateral diffusion can be obtained. By using the new structure with the additional mask layer, the vertical sidewall depth will be more easily extended.

V. Conclusion

A novel wet-etching method for $LiNbO_3$ using an electric-field-assisted proton exchange which has been successfully used is presented in this paper. By applying voltage with appropriate polarity on designed electrodes, the resultant electric field can effectively counteract the proton lateral diffusion caused by the concentration gradient and enhance the proton diffusion rate in the depth direction. Since the proton-exchanged region can be removed by immersing the substrate in an HF/HNO_3 mixture, the proposed wet-etching method can effectively control the shape of the etched region in $LiNbO_3$ substrate. Experimental results by SEM and AFM show that the etching surface is very smooth and the sidewall near the substrate surface is vertical. To the authors' knowledge, these two characteristics have not been achieved by the present dry- and wet- etching techniques at the same time yet. At the applied voltage of 300 V, the vertical sidewall depth reaches 1.23 μm, which is over one half of the total etching depth (2.35 μm). With an increase of the applied voltage, the vertical sidewall depth grows initially at a larger rate and then at a slower rate, which is supposedly due to the accumulation of lithium ion on the boundary of the proton-exchanged region. This situation can be improved by immersing the bottom electrode in the melt of benzoic acid to provide an exit for lithium ions. Increasing the applied voltage, thinning the substrate thickness, and improving the electrode design can further increase the vertical sidewall depth. The proposed wet-etching method has advantages, such as smooth etching surface, adequate etching depth, vertical sidewall, and inexpensive experimental setup. In addition, it satisfies all the requirement of the fabrication process for reflection mirrors and T-junctions. Utilizing the proposed wet-etching method, optical integrated circuits with higher integration density can be fabricated in $LiNbO_3$.

References

[1] P. Buchmann and H. Kaufmann, "GaAs single-mode rib waveguide with reactive ion-etched totally reflecting corner mirrors," *J. Lightwave Technol.*, vol. 3, pp. 785–788, Apr. 1985.

[2] J. E. Johnson and C. L. Tang, "Precise determination of turning mirror loss using GaAs/AlGaAs lasers with up to ten 90° intracavity turning mirrors," *IEEE Photon. Technol. Lett.*, vol. 4, pp. 24–26, Jan. 1992.

[3] L. H. Spiekman, Y. S. Oei, E. G. Metaal, F. H. Groen, P. Demeester, and M. K. Smit, "Ultrasmall waveguide bends: The corner mirrors of the future," *Proc. Inst. Elect. Eng.—Optoelectron.*, vol. 142, no. 1, pp. 61–65, Feb. 1995.

[4] Y. Chung and N. Dagli, "Experimental and theoretical study of turning mirrors and beam splitters with optimized waveguide structures," *Opt. Quantum Electron.*, vol. 27, pp. 395–403, 1995.

[5] H. Han, D. V. Forbes, and J. J. Coleman, "Self-aligned high-quality total internal reflection mirrors," *IEEE Photon. Technol. Lett.*, vol. 7, pp. 899–901, Aug. 1995.

[6] L. Faustini, C. Coriasso, A. Stano, C. Cacciatore, and D. Campi, "Loss analysis and interference effect in semiconductor integrated waveguide turning mirrors," *IEEE Photon. Technol. Lett.*, vol. 8, pp. 1355–1357, Oct. 1996.

[7] S. T. Lau and J. M. Ballantyne, "Two-dimensional analysis of a dielectric waveguide mirror," *J. Lightwave Technol.*, vol. 15, pp. 551–558, Mar. 1997.

[8] R. Orobtchouk, S. Laval, D. Pascal, and A. Koster, "Analysis of integrated optical waveguide mirrors," *J. Lightwave Technol.*, vol. 15, pp. 815–820, May 1997.

[9] R. L. Espinola, R. U. Ahmad, F. Pizzuto, M. J. Steel, and R. M. Osgood Jr., "A study of high-index-contrast 90 degree waveguide bend structures," *Optics Express*, vol. 8, no. 9, pp. 517–528, 2001.

[10] Y. Z. Tang, W. H. Wang, T. Li, and Y. L. Wang, "Integrated waveguide turning mirror in silicon-on-insulator," *IEEE Photon. Technol. Lett.*, vol. 14, pp. 68–70, Jan. 2002.

[11] C. Manolatou, S. G. Johnson, S. Fan, P. R. Villeneuve, H. A. Haus, and J. D. Joannopoulos, "High-density integrated optics," *J. Lightwave Technol.*, vol. 17, pp. 1682–1692, Sept. 1999.

[12] R. U. Ahmad, F. Pizzuto, G. S. Camarda, R. L. Espinola, H. Rao, and R. M. Osgood Jr., "Ultracompact corner-mirrors and T-branches in silicon-on-insulator," *IEEE Photon. Technol. Lett.*, vol. 14, pp. 65–67, Jan. 2002.

[13] Y. Chung, R. Spickermann, D. B. Young, and N. Dagli, "A low-loss beam splitter with an optimized waveguide structure," *IEEE Photon. Technol. Lett.*, vol. 4, pp. 1009–1011, Sept. 1992.

[14] A. Mekis, J. C. Chen, I. Kurland, S. Fan, P. R. Villeneuve, and J. D. Joannopoulos, "High transmission through sharp bends in photonic crystal waveguides," *Phys. Rev. Lett.*, vol. 77, no. 18, pp. 3787–3790, 1996.

[15] C. L. Lee and C. L. Liu, "CF_4 plasma etching on $LiNbO_3$," *Appl. Phys. Lett.*, vol. 35, pp. 756–758, 1979.
[16] Y. Ohmachi and J. Noda, "Electro-optic light modulator with branched ridge waveguide," *Appl. Phys. Lett.*, vol. 27, pp. 544–546, 1975.
[17] J. L. Jackel, R. E. Howard, E. L. Hu, and S. P. Lyman, "Reactive ion etching of $LiNbO_3$," *Appl. Phys. Lett.*, vol. 38, pp. 907–909, 1981.
[18] F. Laurell, J. Webjörn, G. Arvidsson, and J. Holmberg, "Wet etching of proton-exchanged lithium niobate – A novel processing technique," *J. Lightwave Technol.*, vol. 10, pp. 1606–1609, Nov. 1992.
[19] H. J. Lee and S. Y. Shin, "Lithium niobate ridge waveguides fabricated by wet etching," *Electron. Lett.*, vol. 31, no. 4, pp. 268–269, Feb. 1995.
[20] R. S. Cheng, T. J. Wang, and W. S. Wang, "Wet-etched ridge waveguides in Y-cut lithium niobate," *J. Lightwave Technol.*, vol. 15, pp. 1880–1887, Oct. 1997.
[21] S. J. Chung, C. L. Tsai, Y. B. Lin, J. F. Liu, and W. S. Wang, "Improved electrooptic modulator with ridge structure in X-cut $LiNbO_3$," *J. Lightwave Technol.*, vol. 17, pp. 843–847, May 1999.
[22] A. Himeno, H. Terui, and M. Kobayashi, "Loss measurement and analysis high-silica reflection bending optical waveguides," *J. Lightwave Technol.*, vol. 6, pp. 41–46, Jan. 1988.
[23] S. M. Lee, W. C. Chew, M. Moghaddam, M. A. Nasir, S. L. Chuang, R. W. Herrick, and C. L. Balestra, "Modeling of rough-surface effects in an optical turning mirror using the finite-difference time-domain method," *J. Lightwave Technol.*, vol. 9, pp. 1471–1479, Nov. 1991.
[24] S. T. Lau and J. M. Ballantyne, "Two-dimensional analysis of a dielectric waveguide mirror," *J. Lightwave Technol.*, vol. 15, pp. 551–558, Mar. 1997.
[25] R. Orobtchouk, S. Laval, D. Pascal, and A. Koster, "Analysis of integrated optical waveguide mirrors," *J. Lightwave Technol.*, vol. 15, pp. 815–820, May 1997.
[26] S. Wiechmann, H. J. Heider, and J. Müller, "Analysis and design of integrated optical mirrors in planar waveguide technology," *J. Lightwave Technol.*, vol. 21, pp. 1584–1590, June 2003.
[27] J. W. Park, Y. Beak, J. H. Song, E. D. Sim, S. B. Kim, and K. H. Park, "Attenuation characteristics of InP/InGaAsP deep-ridge waveguide turning mirror," *Microwave and Optical Technol. Lett.*, vol. 37, no. 6, pp. 428–431, June 2003.
[28] K. Kawano, K. Noguchi, T. Kitoh, and H. Miyazawa, "A finite element method (FEM) analysis of a shield velocity-matched Ti:$LiNbO_3$ optical modulator," *IEEE Photon. Technol. Lett.*, vol. 3, pp. 919–921, Oct. 1991.

Tzyy-Jiann Wang (M'02) was born in Taichung, Taiwan, R.O.C., in 1970. He received the B.S. and Ph.D. degrees in electrical engineering from National Taiwan University, Taipei, in 1992 and 1999, respectively.

He is currently an Assistant Professor in the Institute of Electro-Optical Engineering, National Taipei University of Technology, Taipei, Taiwan, R.O.C. His research interest includes integrated-optic devices, biosensors, and polymer light-emitting devices.

Chih-Feng Huang was born in Kaohsiung, Taiwan, R.O.C., on March 16, 1978. He received the B.S. degree in electrical engineering from Chinese Culture University, Taipei, Taiwan, R.O.C., in 2000 and the M.S. degree in electrooptical engineering from National Taipei University of Technology, Taipei, Taiwan, R.O.C., in 2002.

His research interest is the design and fabrication of integrated optic devices.

Way-Seen Wang (M'84) was born in Taipei, Taiwan, R.O.C., on March 11, 1948. He received the B.S. degree in electrical engineering from National Taiwan University, Taipei, in 1970 and the M.S. and Ph.D. degrees from the University of Southern California, Los Angeles, in 1975 and 1979, respectively.

Since August 1971, he has been with the Department of Electrical Engineering, National Taiwan University. In 1984, he became a Full Professor. His current research interest includes the design and fabrication of integrated optical waveguide devices.

Pei-Kuen Wei, photograph and biography not available at the time of publication.